AJBAR Vol 1(1), 2022: 109-132, ISSN: 2811-2881

Arid Zone Journal of Basic and Applied Research

Faculty of Science, Borno State University
Maiduguri, Nigeria

Journal homepage: https://www.azjournalbar.com

Research Article

# Transition Metal Complexes Derived From 1*H*-Imidazole Ligand: Synthesis, Characterization, Cyclic Voltammetric Studies and *In Vitro* Antibacterial Evaluation

[1*]Waziri I., [1]Fugu M. B., [2]Zarma H. A., [3]Isa B., and [1]Askira N.K

[1]Department of Pure and Applied Chemistry, University of Maiduguri, P.M.B. 1069, Maiduguri

[2]Department of Biochemistry, University of Maiduguri, P.M.B. 1069, Maiduguri

[3]Department of Chemistry, Borno state University, P.M.B. 1122, Maiduguri.

*Corresponding Author: triumph2236@gmail.com

**ARTICLE INFO:**

**Keyword:**
Complexes.
Coordination chemistry,
Heterocyclic,
Imidazole,
Transition metals.

**ABSTRACT**

Metal complexes consist of metal ions chelated by a group of oppositely charged ions or neutral ligands. These compounds have various applications in stereochemistry, spectroscopy, catalysis, electrochemistry, agriculture, and the medical field; all play some significant roles. This work reports the complexes of $Cr^{3+}$, $Co^{2+}$, and $Zn^{2+}$ metal ions derived from a 1*H*-imidazole ligand system. The complexes were characterized using EA, conductivity measurement, UV-Vis, FTIR, TGA, PXRD, HRMS, SEM-EDX, and $^{1}H$ and $^{13}C\{H\}$NMR for the $Zn^{2+}$ complex. Based on these characterizations, the ligand was found to act as a monodentate and formed a complex with the metal ions *via* a nitrogen atom. An octahedral geometry was obtained for $Cr^{3+}$ and $Co^{2+}$, with composition as $[Cr(IM)_4(H_2O)_2](NO_3)_3$ and $[Co(IM)_6]Cl_2$, and tetrahedral geometry for $Zn^{2+}$ as $[Zn(IM)_2(H_2O)_2]$. Redox conduct of the free chelate and the complexes was studied using cyclic voltammetry (CV). The result showed that $Cr^{3+}$ and $Co^{2+}$ compounds displayed a reductive wave of a one-electron irreversible system for $Cr^{3+}$ to $Cr^{2+}$ and $Co^{2+}$ to $Co^{+}$. The ligand shows a comparable electrochemical response to $Cr^{3+}$ and $Co^{2+}$ complexes with a reduction peak denoting a reduction involving one-electron transfer, while the $Zn^{2+}$ complex shows neither oxidative nor reductive waves. The free ligand and the complexes were evaluated for antimicrobial activity against Gram-positive: (*Staphylococcus aureus* and *Streptococcus pyogenes*) and Gram-negative: (*Escherichia coli* and *Klebsiella pneumoniae*). From the result obtained, the complexes demonstrated enhanced activity compared to the ligand. The order of the activities among complexes on the organisms can be arranged as follows: $Co^{2+} > Cr^{3+} > Zn^{2+}$.

**Corresponding author**: Ibrahim Waziri, Email: triumph2236@gmail.com
Department of Pure and Applied Chemistry, University of Maiduguri.

## INTRODUCTION

Heterocyclic compounds belong to the group of versatile ligands that are of great importance in coordination chemistry (Chen, 2016). Heterocyclic compounds form sturdy metal complexes with most metallic elements within the periodic table under certain conditions (Andersson Trojer, Movahedi, Blanck, & Nydén, 2013). These ligands and their complexes are in stereochemistry, structure, spectroscopy, coordination chemistry, catalysis, analytical chemistry, photochemistry, electrochemistry, agriculture, medical fields; they all play an important role (Basner, 2017; Yan et al., 2017). The most common and frequently used heterocyclic ligand in coordination chemistry is 2,2'-bipyridine (Constable & Housecroft, 2019; Pal, 2018). The 2,2'-bipyridine complex was first reported as tris (2,2 '-bipyridine) ruthenium in 1939 by Burstall, but the properties and application of this compound were realized in 1959 after a spectroscopic investigation by Paris and Brandt (Bhuiyan, Kudo, & Bartlett, 2010; Richardson, 1999). Since then, heterocyclic ligands have arguably become the most studied and used ligands in coordination chemistry (Davison, 2014).

In search for complex compounds with the better therapeutic application, and to address the growing needs of pharmaceutical industries and scientific research, other heterocyclic compounds such as pyrazole, imidazole, 1,2,4-triazole, and tetrazole systems have been incorporated into ligands (Kerru, Gummidi, Maddila, Gangu, & Jonnalagadda, 2020). Although, these have not been studied in much detail as the 2,2'-bipyridine ligands. These ligands form complexes with unique properties different from 2,2'-bipyridine owing to their other electronic properties (Bai, Young, & Hor, 2011; Fischer, 2010; Qi & Wang, 2014). Due to the electron-rich properties of these azoles ligands over azines, this work focus on imidazole as a ligand of choice for coordination with some selected transition metals specifically with 1*H*-imidazole (Figure 1).

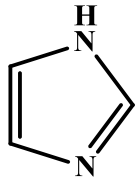


**Figure 1**: Structure of 1*H*-imidazole

1*H*-imidazole is a five-membered ring organic molecule containing two conjugated pie bonds and two nitrogen atoms suitable for coordination. Together with its other derivatives, this molecule has been utilized as magnificent contenders for the design of metals hybrids molecules in the discipline of coordination chemistry (Chen, 2016). The chemistry of imidazole has gained attention owing to its promising application in biological systems (Sandbhor et al., 2004). It has wide applications in the pharmaceutical industry as an antifungal agent. Various researches also show its application as a catalyst in the synthesis of copolymer, anisotropic conductor, and electron acceptor in charge-transfer solid (Erden, Demirhan, & Avcıata, 2006).

We reported the synthesis and characterization of $Cr^{3+}$, $Co^{2+}$ and $Zn^{2+}$ complexes with a 1*H*-imidazole ligand system. The stoichiometry of the complexes was confirmed using EA analysis, FTIR, UV-visible, HRMS, PXRD, TGA, SEM-EDX, and $^{1}$H NMR and $^{13}$C{H}NMR for the free ligand and the $Zn^{2+}$ complex. Cyclic voltammetry study and biological evaluation were performed on all the compounds.

## EXPERIMENTAL

### Materials and methods

All chemicals and reagents utilized were analytical grade (AR) and purchased from Sisco Research Laboratories (SRL) Pvt Ltd or Sigma-

Aldrich. They were used as obtained without further purification or modification unless otherwise stated. These include: 1*H*-imidazole, MeOH, EtOH, DMSO, DMF, ACN, $Cr(NO_3).9H_2O$, $CoCl_2.6H_2O$, and $Zn(NO_3)_2.6H_2O$.

**General procedure for the synthesis of the complexes**

Methanolic solutions 20 mL of each metal salt: ($Cr(NO_3)_3.9H_2O$, 0.4002 g, 1 mmol, 1 eq), ($CoCl_2.6H_2O$, 0.2379 g, 1 mmol, 1 eq) and ($Zn(NO_3)_3.6H_2O$, 0.1894 g, 1 mmol, 1 eq) was added to methanolic solution 10 mL of the ligand (0.0680 g, 1 mmol, 1eq) in the mole ratio of 1:1; the solution was stirred at room temperature (25 ˚C) until precipitates of the complexes were formed (Sumrra, 2021), **scheme 1.** The formed product was filtered, washed with methanol, ether, and dried over phosphorus oxide ($P_2O_5$).

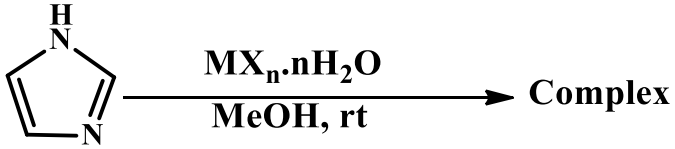


**Scheme 1:** General procedure for the synthesis of the complexes: M = Cr (III), Co (II) or Zn (II); X = $NO_3$ or $Cl_2$; n = 2, 3, 6 or 9

**$[Cr(IM)_4(H_2O)_2](NO_3)_3$**

Yield: 62 % (0.2315 g); dark green solid; m.p. 225–230 ˚C (decomp); $IR_{ATR}$; $cm^{-1}$: 3278 (OH); 2974 (NH); 1346 (CN); 1064 (C-H); 551 (Cr-O); 474 (Cr-N); UV-Vis. (DMSO, nm): 305, 398, 480; CHN Anal. Calculated for $C_{12}H_{20}CrN_{11}O_{11}$: C, 26, 38; H, 3.69; N, 28.20; found: C, 26.35; H, 3.58; N, 28.16; HRMS-ESI *m/z* $[M-H]^-$ 546.8404 (Calculated for $C_{12}H_{20}C_rN_{11}O_{11}$ 546.0749).

**$[Co(IM)_6]Cl_2$**

Yield: 88 % (0.1007 g); reddish brown solid; m.p. 273–283 ˚C (decomp); $IR_{ATR}$: $cm^{-1}$: 3012 (NH); 1485 (CN); 1076 (C-H); 667 (Co-O); 470 (Co-N); UV-Vis. (DMSO, nm): 299, 406, 476; CHN Anal. Calculated for $C_{18}H_{24}Cl_2CoN_{12}$: C, 40.16; H, 4.49; N, 31.22; found: C, 40.10; H, 4.38; N, 31.17; HRMS-ESI *m/z* $[M+H]^+$ 538.2079 (Calculated for $C_{18}H_{24}Cl_2CoN_{12}$ 538.0956)

**$[Zn(IM)_2(H_2O)_2]$**

Yield: 82 % (0.1237 g); white solid; m.p. 283–286 ˚C (decomp); $^1H$ NMR (500 MHz, DMSO-$d_6$): δ (ppm) = 7.20 (s, 2H), 8.01 (s, 1H); $^{13}C\{H\}$NMR (125 MHz, DMSO-$d_6$): δ (ppm) = 121.8, 135.3 (2C); $IR_{ATR}$: $cm^{-1}$: 3568 (OH); 1489 (CN); 1087 (C-H); 597 (Zn-O); 470 (Zn-N); UV-Vis. (DMSO, nm): 259; 381; CHN Anal. Calculated for $C_6H_{10}N_4O_2Zn$: C, 30.59; H, 4.28; N, 23.79; found: C, 30.57; H, 4.22; N, 23.72; HRMS-ESI *m/z* $[M-H]^-$ 234.9288 (Calculated for $C_6H_{10}N_4O_2Zn$ 234.0095)

**Measurements**

All the measurements were conducted on the free ligand and the synthesised complexes. The proton nuclear magnetic resonance ($^1H$ NMR) spectra were recorded on Bruker 500 MHz spectrometer, and carbon nuclear magnetic resonance ($^{13}C\{H\}$NMR) were performed with Bruker 125 MHz spectrometers. Infrared spectra were recorded using Tensor 27 Bruker and Perking Elmer Fourier Transformed Infra-red (FTIR) spectrometer BX in the range of (4000–400 $cm^{-1}$). Elemental analyses were carried out on a VarioElementar III microbe CHN analyser. All NMR analyses were conducted at room temperature. The chemical shifts are reported as

parts per million (ppm) relative to tetramethylsilane, which is used as internal standards for $^{1}H$ NMR and $^{13}C\{H\}$NMR for DMSO. High-resolution mass spectra (HRMS) were performed on a WatersAcquity UPLC Synapt G2 HD mass spectrometer. Thermogravimetric analyses (TGA) were performed on a TGA-Q600 thermo-analyser with a heating rate of 10 $^{\circ}C\ min^{-1}$ under $N_2$ flow (20 mL/min) at a temperature range of 25 to 800 ˚C. The metal content in the complexes was determined using a Spectro Arco FSH12 inductively-coupled plasma mass spectrometry. Powder X-ray diffraction (PXRD) data were collected at 40 KeV, 15 mA on a RigakuMiniFlex 600 Benchtop diffraction using Cu-Kα radiation (ƛ = 1.5418Å) over a 2θ range of 0-80 ˚C at room temperature. Scanning electron microscope (SEM) coupled with energy dispersive X-ray diffraction spectroscopy (EDX) was used to determine the morphology and elemental composition of the complexes.

**Electrochemical study (cyclic voltammetry)**

A Biologic SP-200 Computer-controlled electrochemical measurement device with a potentiostat was used to perform the electrochemical measurements. A working electrode (glassy carbon), a counter electrode (platinum wire), and a saturated Ag/AgCl in KCl as a reference electrode comprised a three-electrode system. A 0.01 M solution of phosphate buffer solution (PBS) pH 7.4 was utilized during the electrochemical studies as a supporting electrolyte (Alzahrani et al., 2020).

**Antimicrobial studies**

The synthesised complexes and the free ligand were screened for their anti-microbial activity on Gram-positive: (*Staphylococcus aureus* ATCC-25923 (Sa), *Streptococcus pyrogens* ATCC-19615 (Sp), Gram-negative: (*Escherichia coli* ATCC-25922 (Ea), and *Klebsiella pneumoniae* ATCC-13883 (Kp)), using *in vitro* disc diffusion method in DMSO as a solvent (Othman, Gad-Elkareem, El-Naggar, Nossier, & Amr, 2019). ciprofloxacin was utilized as a reference drug. The zone of inhibition obtained for each compound against the tested organisms was measured in triplicate, and the results are presented as mean ± SD.

## RESULTS AND DISCUSSION

**Physico-chemical properties**

The ligand used in this study (1*H*-imidazole) was ascertained using: $^{1}H$ NMR, $^{13}C\{H\}$NMR, IR, UV-Vis, HRMS, TGA, and CHN analysis before complexing it with the metal ions. The synthesised metal complexes are microcrystalline, except $Cr^{3+,}$ which is amorphous. The compounds were found to be insoluble in acetone, benzene, hexane and chloroform but soluble in DMSO, DMF, ACN, and EtOH. Their solubility in these polar solvents suggests that the compounds are probably polar. The complexes were obtained in good yield (62-88). They are air and light stable and decompose within the range of 225–286 ˚C. The molar conductivity values in (DMSO, $10^{-3}$ M) were found to be within the range of (12.56–17.93) $\Omega^{-1}\ cm^2\ mol^{-1}$, unveiling weak electrolytic property (Tyagi, Chandra, Saraswat, & Yadav, 2015).The result of the CHN analyses on the free ligand and the complexes fit well with the stoichiometric of the compounds and also correlate with the calculated values. The physicochemical and analytical data of the compounds are presented in Table 1.

**Table 1:** Physico-chemical properties of the ligand and its complexes

| Compound | Molecular formula (Molecular weight) | Colour | Yield % (g) | m.p./d.p (˚C) | Elemental analysis: Calc. (found) | | | | Molar conductivity ($\Omega^{-1}cm^2mol^{-1}$) |
|---|---|---|---|---|---|---|---|---|---|
| | | | | | C | H | N | M | |
| IM | $C_3H_4N_2$ (68.0374) | Colorless | - | 92 | 52.93 (52.93) | 5.92 (5.92) | 41.15 (41.14) | - | - |
| $[Cr(IM)_4(H_2O)_2](NO_3)_3$ | $C_{12}H_{20}CrN_{11}O_{11}$ (546.8404) | Dark green | 62 (0.2315) | 225-231 | 26.38 (26.33) | 3.69 (3.58) | 28.20 (28.16) | 9.52 (9.49) | 17.93 |
| $[Co(IM)_6]Cl_2$ | $C_{18}H_{24}Cl_2CoN_{12}$ (538.2097) | Reddish brown | 88 (0.1007) | 271-278 | 40.16 (40.10) | 4.49 (4.38) | 31.22 (31.17) | 10.95 (10.93) | 14.48 |
| $[Zn(IM)_2(H_2O)_2]$ | $C_6H_{10}N_4O_2Zn$ (234.9288) | white | 82 (0.1237) | 283-286 | 30.59 (30.57) | 4.28 (4.22) | 23.79 (23.72) | 27.76 (27.74) | 12.56 |

**IM = 1*H*-imidazole; m.p. = Melting point; d.p. = Decomposition point; Calc. = Calculated; g = Grams; M = Cr, Co and Zn**

**$^{1}$H and $^{13}$C{H}NMR**

The $^{1}$H and $^{13}$C{H}NMR could not be perform on the complexes of $Cr^{3+}$ and $Co^{2+}$ due to their paramagnetic nature as the result of unpaired electrons in their d-orbital. However, the $^{1}$H and $^{13}$C{H}NMR of the free ligand and the $Zn^{2+}$ complex in DMSO-$d_6$ were obtained, and the spectra are presented in Figure: 1–4. The $^{1}$H NMR of the free ligand displayed three distinct peaks, and these peaks account for all the protons in the molecule. The imidazole proton appeared downfield at 12.04 ppm as broad peak. The appearance of this proton in the downfield region is due to the influence of withdrawing electron from nitrogen atoms which causes a decrease in the electron density at the proton nucleus. This resulted in the deshielding of the proton nucleus, causing a larger chemical shift downfield. The two singlet peaks at 7.02 ppm and 7.64 ppm represent the C-H protons in the imidazole ring. The peak at 7.02 ppm is for the equivalent protons in positions 4 and 5 in the imidazole ring, and the proton at position 2 appeared at 7.64 ppm. After complexation to the $Zn^{2+}$ ion, and as shown in the $^{1}$H NMR spectrum of the $Zn^{2+}$ complex (Figure 3), the imidazole proton that appeared downfield at 12.04 ppm in free ligand didn't appear on the spectrum of the complex. The disappearance of this proton in the complex justified the displacement of the imidazole proton and coordination of the $Zn^{2+}$ ion to the ligand *via* the deprotonated nitrogen atom. Similarly, both protons at positions 4 and 5 that appeared at 7.64 ppm and 7.02 ppm in the spectrum ligand reappeared but shifted downfield to 8.01 ppm and 7.20 ppm, respectively. This shift results from the deprotonation of the imidazole proton and following the reaction of the metal ion to the ligand via the nitrogen atom, which causes more decrease in the electron density at the nucleus of the protons with an increase in the deshielding effect. There is also the appearance of a broad peak at 3.32 ppm on the complex spectrum, which is due to the moisture content of the DMSO-$d_6$ used for the NMR. The $^{13}$C{H}NMR of the free ligand showed two peaks at 135 .2 ppm, which is due to the carbons at positions 4 and 5, and a peak at 121.7 ppm for the carbon at position 2. After coordinating to the $Zn^{2+}$ ion, the peak at 135.2 ppm shifted to upfield at 119.7 ppm, and the peak at 121.7 ppm shifted to downfield at 134.3 ppm. This significant shift in the positions of both the proton and carbon, with the disappearance of the N-H proton, confirmed the complex's formation.

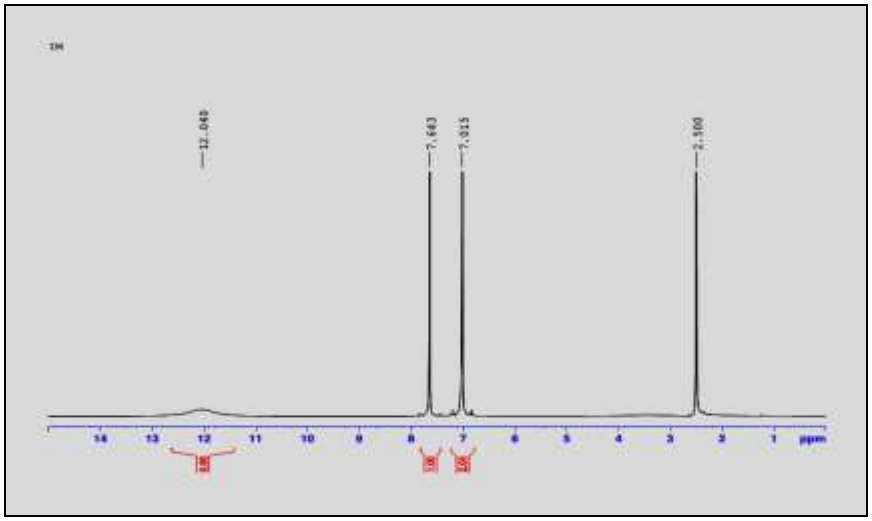


**Figure 1:** $^{1}$H NMR spectrum of the ligand, (500 MHz, DMSO-$d_6$)

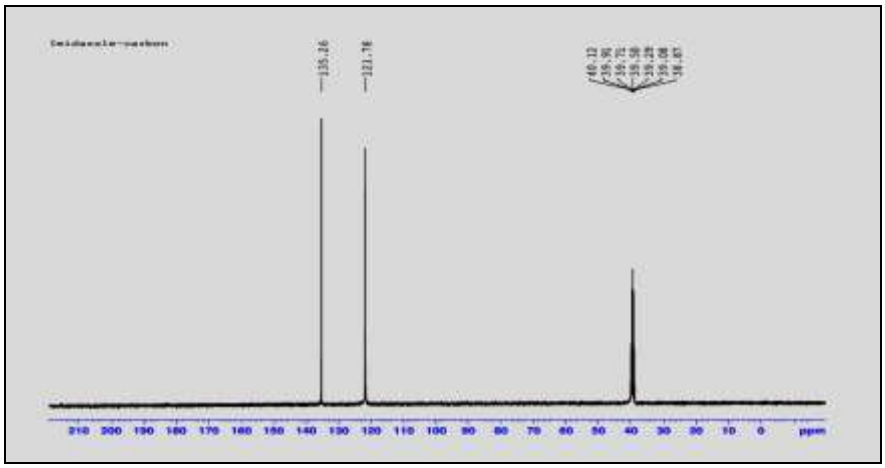

**Figure 2:** $^{13}C\{H\}NMR$ spectrum of the ligand, (500 MHz, DMSO-$d_6$)

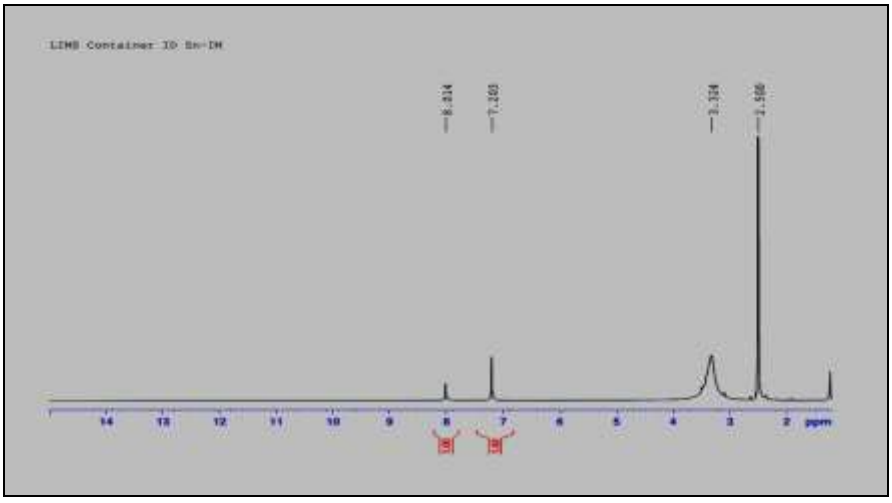

**Figure 3:** $^{1}H$ NMR spectrum of $[Zn(IM)_2(H_2O)_2]$, (500 MHz, DMSO-$d_6$)

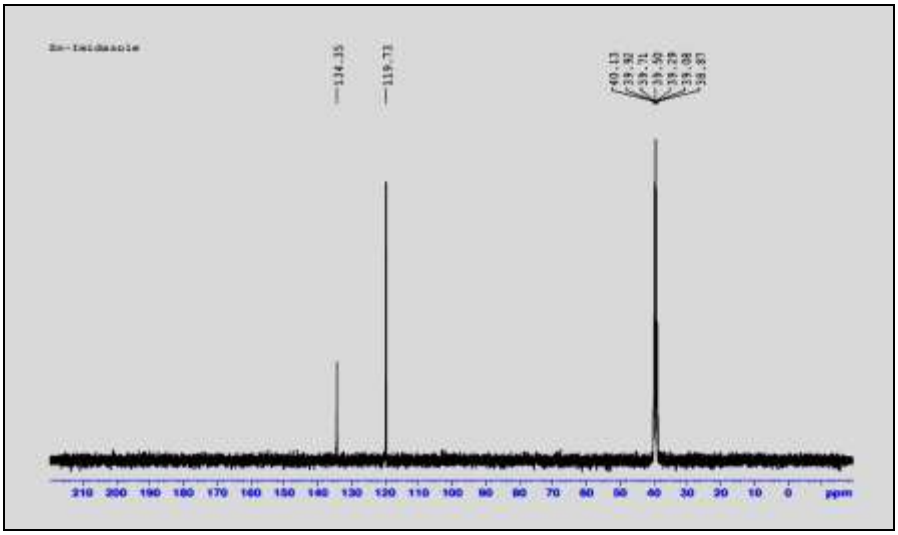

**Figure 4:** $^{13}C\{H\}NMR$ spectrum of $[Zn(IM)_2(H_2O)_2]$, (500 MHz, DMSO-$d_6$)

**Infrared spectra**

Infrared spectroscopy is an important tool used in coordination chemistry to confirm the formation of complexes. To ascertain the formation of a complex, the infrared spectrum of a free ligand is compared with that of the complex (Sridharan, 2016). Herein, the infrared spectra of the 1*H*- imidazole ligand and the complexes were obtained in the region of 4000–500 $cm^{-1}$. The data is recorded in Table 2, and the spectra are presented in Figure 5.

**Table 2:** Infrared spectral data ($cm^{-1}$) of the ligand and its complexes

| Compound | υ(O-H) | υ(N-H) | υ(C-N) | υ(C=C) | υ(M-O) | υ(M-N) |
|---|---|---|---|---|---|---|
| IM | – | 3020 | 1446 | 1045 | – | – |
| $[Cr(IM)_4(H_2O)_2](NO_3)_3$ | 3278 | 2974 | 1346 | 1064 | 551 | 474 |
| $[Co(IM)_6]Cl_2$ | – | 3012 | 1485 | 1076 | – | 470 |
| $[Zn(IM)_2(H_2O)_2]$ | 3568 | – | 1489 | 1087 | 597 | 470 |

The spectrum of the free ligand displayed a strong absorption band at 3020 $cm^{-1,}$ which can be attributed to the N-H stretching frequency (Trivedi *et al.,* 2018; Uluçam & Turkyilmaz, 2018). This stretching frequency changed to a lower wave number in the spectra of $Cr^{3+}$ and $Co^{2+}$, and disappeared in the spectrum of $Zn^{2+}$ complex. The disappearance of this band in the spectrum of the $Zn^{2+}$ complex rectifies the disappearance of the imidazole proton and coordination of the zinc ion to the ligand via the nitrogen atom, which is also evident from the $^1H$ NMR of the complex. Furthermore, the change in the position of this band to another wave number (lower) in $Cr^{3+}$ and $Co^{2+}$ complexes is due to the molecule's vibration as the result of coordination of the metal ion to the ligand via the second nitrogen atom. The emergence of a new band in all the complexes in the region of (470-474) $cm^{-1}$ which is assignable to the metal-nitrogen band as reported in the literature (Ding, Wang, Kou, Li, & Shi, 2019; Hashem, Mohamed, Farag, Negm, & Azmy, 2021; Tyagi *et al.,* 2015), further confirmed the formation of the complexes. The band at 1446 and 1045 $cm^{-1}$ in the free ligand are due to C-N and C=C, respectively (Alamanova *et al.,* 2021). The C-N band shifted to the region 1346-1489 $cm^{-1}$ in the complexes, and C=C bands were observed within (1064-1087) $cm^{-1}$. These shifts are attributed to the vibration of the molecules due to the complexation of the metal ions to the ligands. In addition, evidence of coordinated water molecules in $Cr^{3+}$ and $Zn^{2+}$ complexes was confirmed by the appearance of broad band at 3278 $cm^{-1}$ and 3568 $cm^{-1,}$ respectively. These bands result from intermolecular hydrogen bonding (Hassan, Fayez, & Abdalla, 2020; Karaağaç, 2020). The manifestation of a new band at 551 $cm^{-1}$ in the $Cr^{3+}$ complex and at 597 $cm^{-1}$ in $Zn^{2+}$ which is assignable to the metal-oxygen band, confirmed the presence of water of coordination.

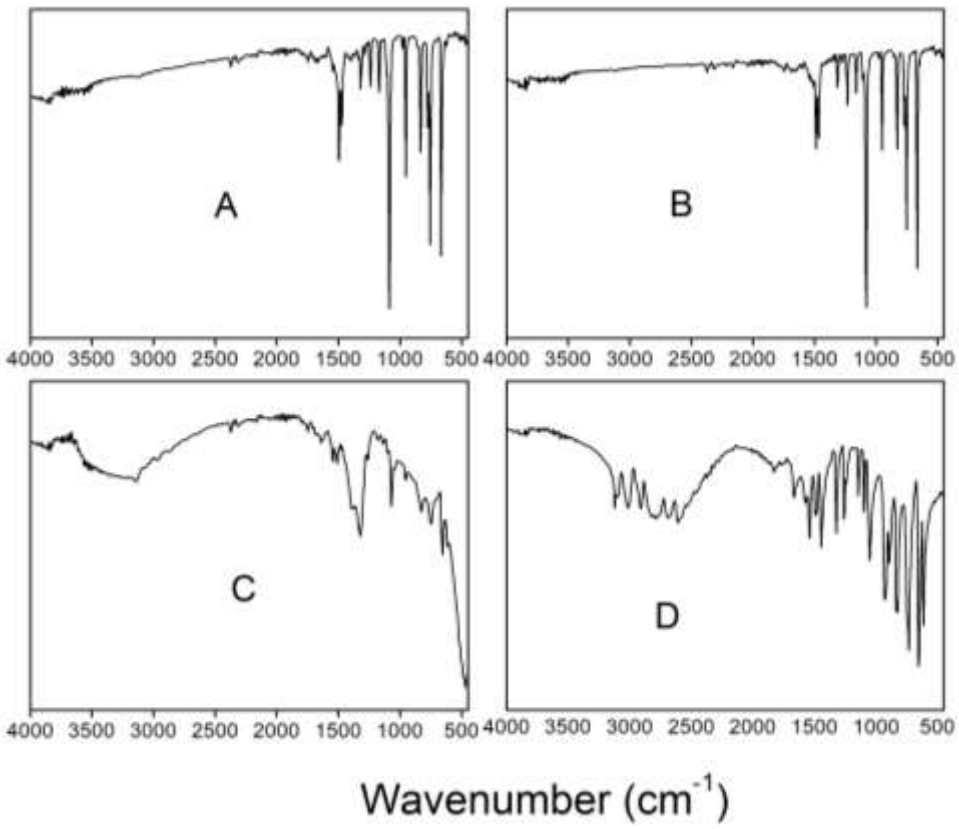


**Figure 5:** The plot of IR spectra of the ligand and its complexes; A = $[Zn(IM)_2(H_2O)_2]$, B =$[Co(IM)_6]Cl_2$, C = $[Cr(IM)_4(H_2O)_2](NO_3)_3$, D = 1*H*-imidazole (ligand)

**Electronic spectral study**

An electronic (UV-Vis) spectral study of metal complexes provides additional insight regarding the nature of coordination between the central atom and the ligands via the vacant orbital of the metal ions. The UV-Vis absorption spectra of the free ligand and the complexes were obtained in DMSO ($10^{-3}$ M) at ambient temperature. The spectral information band assignments with the specific geometries are given in Table 3, and the plot of spectra is shown in Figure 6.

The UV-Vis spectra of the free ligand displayed two absorption peaks in the region of 267 and 309 nm assignable to $\pi \rightarrow \pi^*$ and $n \rightarrow \pi^*$ transition due to C-H, C-C, C=C, and C-N/C=N within the organic moiety of the imidazole ligand. $Cr^{3+}$ complex displayed three peaks at 305, 398, and 520 nm, corresponding to V1, V2, and V3. These peaks are assignable to $^4A_{2g} \rightarrow {}^4T_{1g}(P)$, $^4A_{2g} \rightarrow {}^4T_{1g,}$ and $^4A_2 \rightarrow {}^4T_{2g}$ transition within the octahedral geometry. Similarly, the $Co^{2+}$ complex displayed three distinct peaks at 299, 406, and 476 nm, which can be assigned to $^4T_{1g} \rightarrow {}^4T_{1g}$,(P) $^4T_{1g} \rightarrow {}^4A_{2g}$, and $^4T_{1g} \rightarrow {}^4T_{2g}$, (P) transition with octahedral geometry. The diamagnetic $Zn^{2+}$ complex presented two absorption peaks at 259 and 381 nm. These result from ligand-metal charge transfer (LMCT) within the tetrahedral environment. Similarly, the racah parameters (B) and nephelauxetic ratio (β) of the $Cr^{3+}$ and $Co^{2+}$ complexes were found to be 785 and 993 $cm^{-1,}$ respectively, Table 6. The nephelauxetic ratios (β) of $Cr^{3+}$ complexes were found to be 0.762, and that of $Co^{2+}$ complexes was 0.889, which

indicates the covalency between the metal ions and their ligands. Both the $Cr^{3+}$ and $Co^{2+}$ complexes presented nephelauxetic ratios (β) value of less than one, which is due to the decrease in inter-electronic repulsion from electronic delocalization during the complexation process (Dalal, 2017). Because the nephelauxetic ratios (β) of the free metal ions are more than one. Furthermore, the crystal field splitting energy ($\Delta_o$) of the complexes corresponds to octahedral geometries, Table 3. However, $Zn^{2+}$ complex having tetrahedral geometry with the orbital splitting pattern of $dx^2–y^2$ and $dz^2$ and equally low orbital energy due to the position of the orbital between the ligand axis experiences slight repulsion. Hence, the racah parameters (B), nephelauxetic ratio (β), and crystal field splitting energy ($\Delta_o$) are very minimal and insignificant.

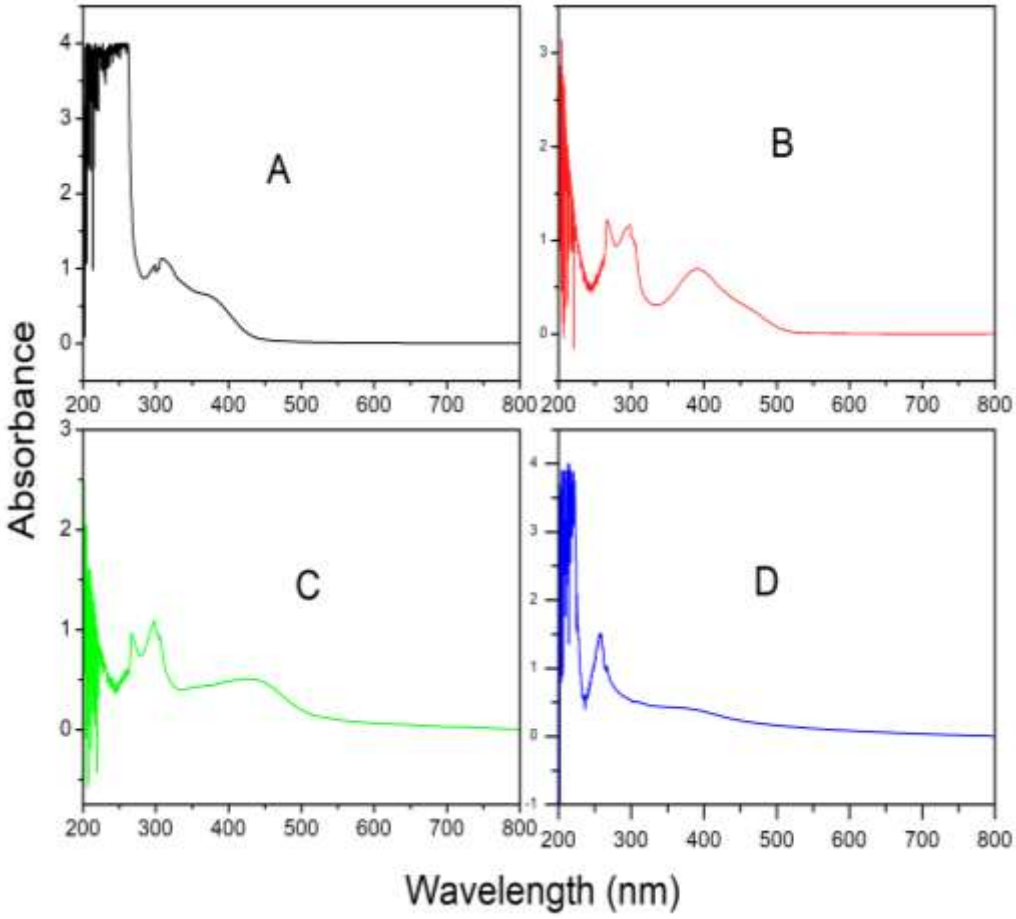


**Figure 6:** Plot of the UV-Vis spectra of the ligand and its complexes. A = 1*H*-imidazole (ligand), B = $[Cr(IM)_4(H_2O)_2](NO_3)_3$, C = $[Co(IM)_6]Cl_2$, D = $[Zn(IM)_2(H_2O)_2]$

**Table 3:** Electronic spectral data of the ligand and the complexes

| Compound | λmax (nm) | Band assignment | B ($cm^{-1}$) | β | V2/V1 | $\Delta_o$ ($cm^{-1}$) | Geometry |
|---|---|---|---|---|---|---|---|
| IM | 269 | $\pi \rightarrow \pi^*$ | | - | - | - | - |
| | 309 | $n \rightarrow \pi^*$ | | | | | |
| $[Cr(IM)_4(H_2O)_2](NO_3)_3$ | 305 | $^4A_{2g} \rightarrow {}^4T_{1g}(P)$ | 785 | 0.762 | 1.31 | 17270 | Octahedral |
| | 398 | $^4A_{2g} \rightarrow {}^4T_{1g}$ | | | | | |
| | 520 | $^4A_2 \rightarrow {}^4T_{2g}$ | | | | | |
| $[Co(IM)_6]Cl_2$ | 267 | $^4T_{1g} \rightarrow {}^4T_{1g}(P)$ | 993 | 0.889 | 1.36 | 9434 | Octahedral |
| | 406 | $^4T_{1g} \rightarrow {}^4A_{2g}$ | | | | | |
| | 476 | $^4T_{1g} \rightarrow {}^4T_{2g}$ | | | | | |
| $[Zn(IM)_2(H_2O)_2]$ | 259 | $\pi \rightarrow \pi^*$ | - | - | 1.47 | - | Tetrahedral |
| | 381 | LMCT | | | | | |

**Powder x-ray diffraction studies**

Several attempts were made toward obtaining a single crystal for SCXD analysis, which was unsuccessful. Hence, powder x-ray diffraction analysis (PXRD) was carried out on the compounds. This is an important tool for identifying and characterizing crystalline or amorphous materials/compounds. Crystalline materials show sharp peaks under powder x-ray diffraction, and amorphous materials or compounds show broad background signals (Gonon, 2020). The free ligand and the complexes were subjected to PXRD analysis, and the diffraction patterns are shown in Figure 7. From the diffraction patterns obtained, it can be seen that the ligand and its $Co^{2+}$ and $Zn^{2+}$ complexes exhibit sharp peaks, and this suggests that they are crystalline. The $Cr^{3+}$ complex exhibits a broad signal, which indicates its amorphous nature. A data search and matches within the database (Cambridge structural database, v.1.18) (Groom, Bruno, Lightfoot, & Ward, 2016), for comparison with data obtained, this work could not unveil the existence of any compound(s) with similar data or closely related. This indicates the non-existence of compound(s) having a similar diffraction pattern reported in the database.

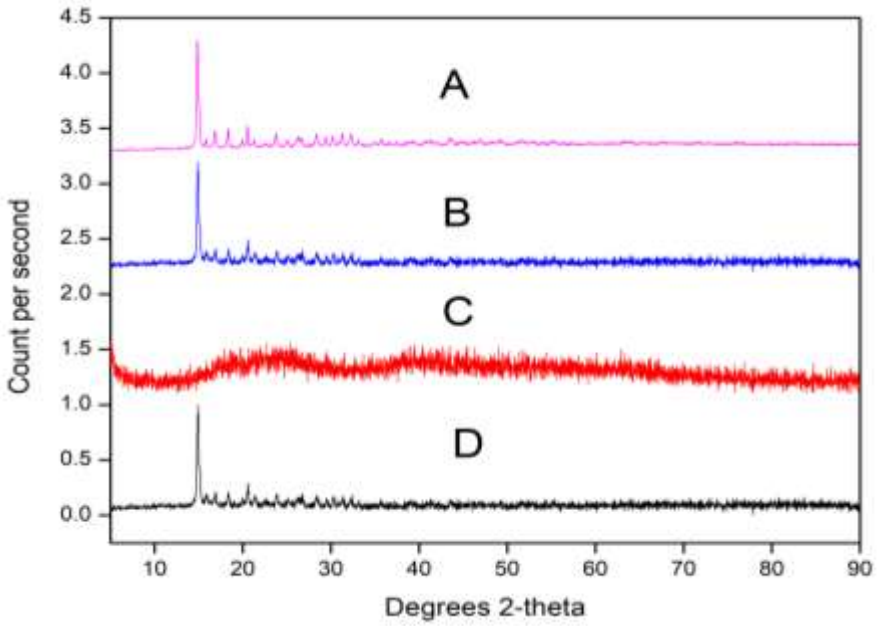


**Figure 7:** The plot of powder x-ray diffraction patterns of the ligand and the complexes. A=$[Zn(IM)_2(H_2O)]$, B= $[Co(IM)_6]Cl_2$, C= $[Cr(IM)_4(H_2O)_2](NO_3)_3$, D = 1*H*-imadazole (ligand)

**Thermal analysis**

To evaluate the effect of heat on the complexes, thermogravimetric analysis (TGA) was performed on the complexes at 25–800 ˚C (Figures: 8-10). The thermal behaviour of the compound at this temperature range showed three decomposition steps. The first decomposition steps at *ca* 25–120 ˚C with weight loss of 7, 14, and 7 %, calculated as 8, 15.4, and 8 %, respectively, represent the loss of water molecules in $Cr^{3+}$ and $Zn^{2+}$ complexes and moisture content in $Co^{2+}$ complex. The second decomposition step represents the decomposition of the organic molecules (ligands). The third and final decomposition step in the

thermogram of all the complexes, as shown in Figures 8-10, represents the formation of metal oxide (residue). These metal oxides are $Cr_2O_3$, CoO, and ZnO, respectively. The fragments are fully accounted for on the mass spectroscopic analysis.

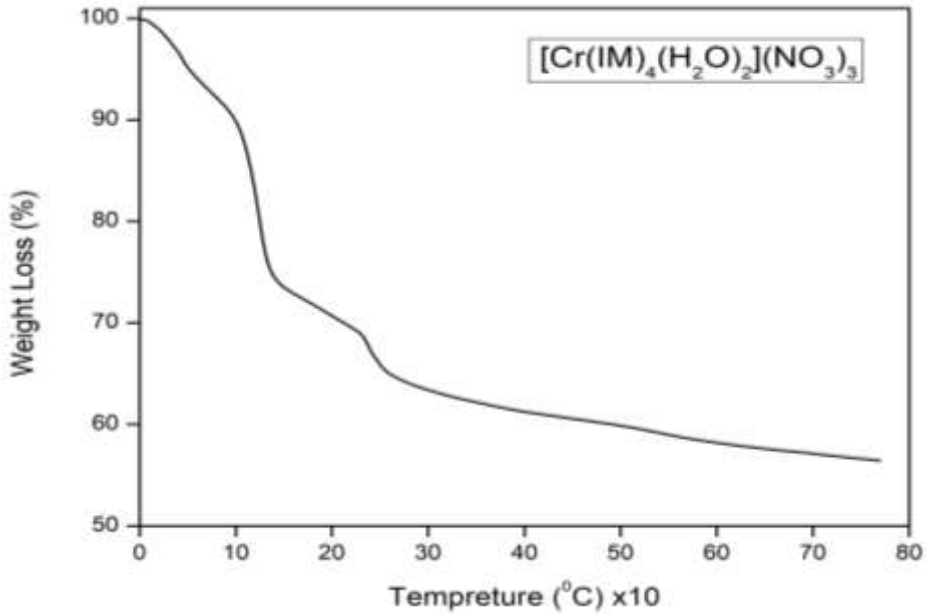


**Figure 8:** The plot of thermogram for $Cr^{3+}$ complex

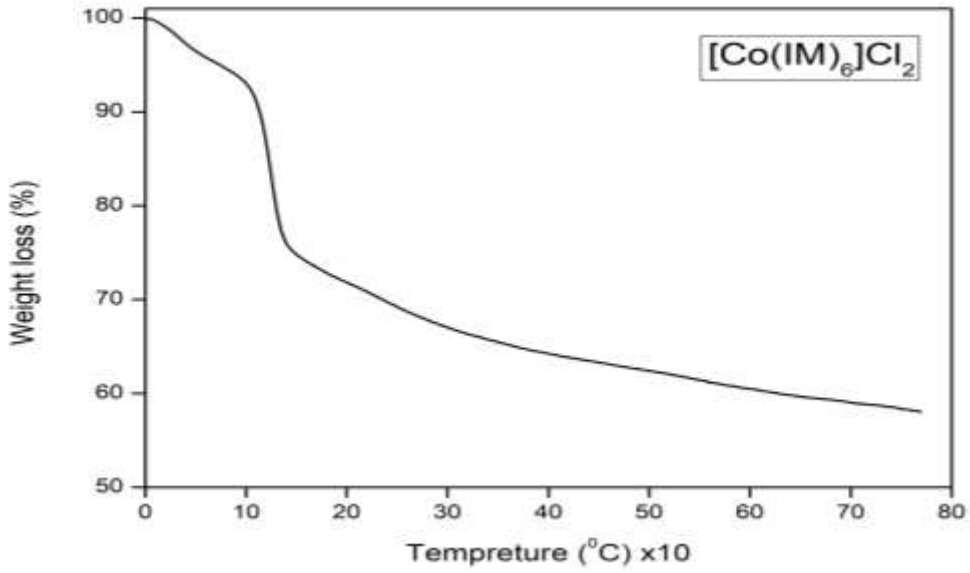


**Figure 9:** The plot of thermogram for $Co^{2+}$ complex

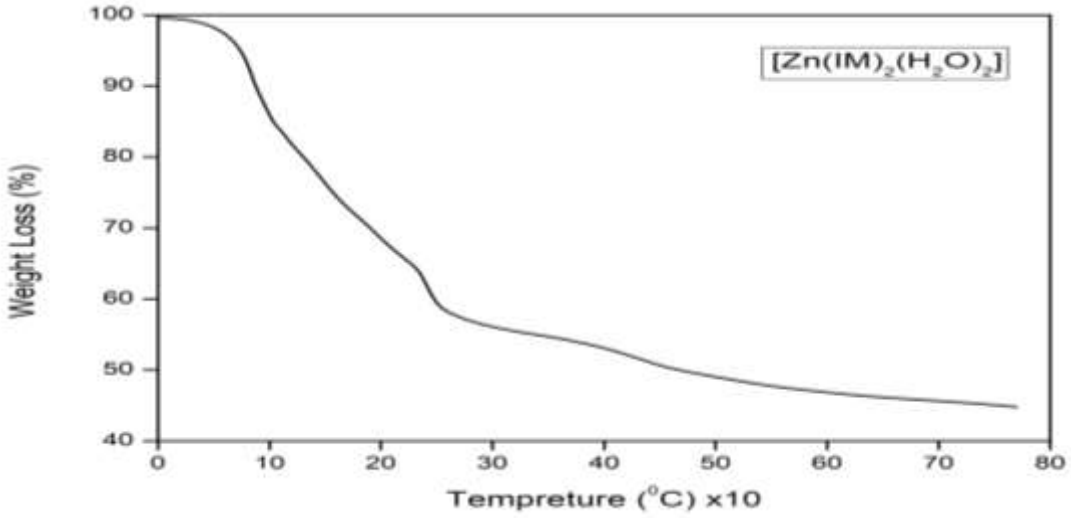


**Figure 10:** The plot of thermogram for $Zn^{2+}$ complex

**Mass spectrometry studies**

To further confirm the formation of the complexes, mass spectral studies were conducted on the free ligand and its complexes, and the spectra are presented in Figures 11–14. A corresponding characteristic peak on the mass spectrum of the free ligand at *m/z* 91.0305 assignable to $[IM+Na]^+$ (100 %), Figure 11. In the spectra of the complexes, the molecular ion peaks $[M]^+$, $[M+H]^+$ and $[M-H]^+$ were observed at *m/z* 538.0989 (100%), 539.0926 (63.9%) and 537.0956 (19.5%) for $Co^{2+}$ complex. Similarly, the fragment observed at *m/z* 218.2256 (16.6 %) is attributed to $[Co(IM)_2Na]$, Figure 12.The mass spectrum of $Cr^{3+}$ complex showed characteristic peaks at *m/z* 546.8404 (100%) and 325.1844 (60%), these are attributed to $[M]^+$ and $[Cr(IM)_4+H]^+$, Figure 13. However, the mass spectrum of $Zn^{2+}$ complex displayed peaks at *m/z* 234.9288 (100%) and 236.9236 (25%), which are attributed to $[M]^+$ and $[M+2]^{2+}$ respectively, Figure 14. The fragments obtained on the spectra of the complexes correlate well with the proposed structures, and thermal analysis studies hence confirmed the formation of the complexes

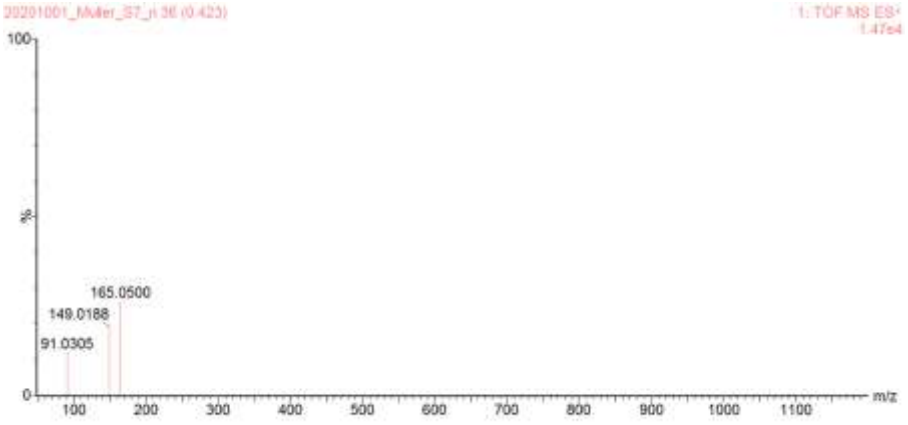


**Figure 11:** Mass of the spectrum of the free ligand (IM)

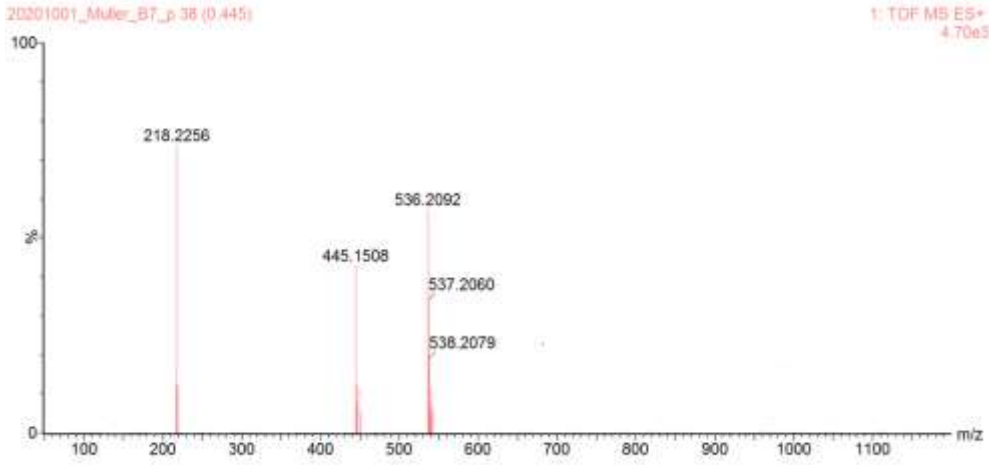


**Figure 12:** Mass spectrum of $[Co(IM)_6]Cl_2$ complex

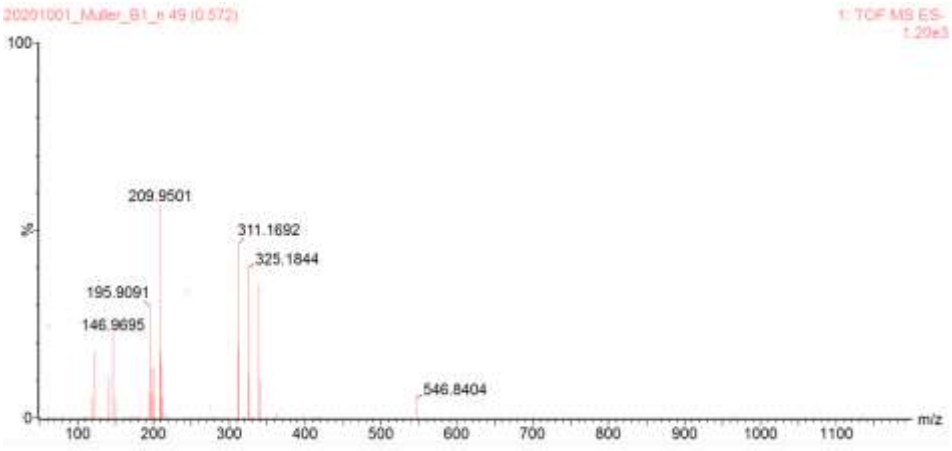


**Figure 13:** Mass spectrum of $[Cr(IM)_2(H_2O)_2]$ complex

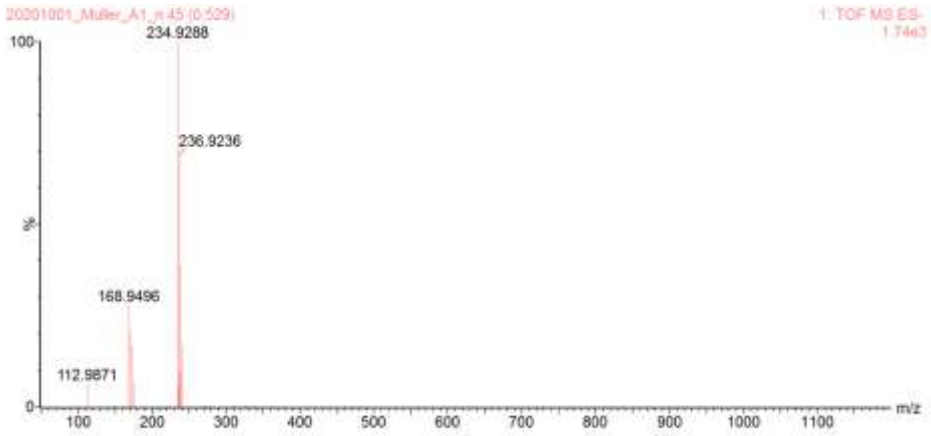


**Figure 14:** Mass spectrum of $[Zn(IM)_2(H_2O)_2]$ complex

**Scanning electron microscopy-energy dispersive x-ray analysis (SEM-EDX)**

To access information regarding the surface arrangement and the chemical composition of the synthesised complexes, the SEM-EDX spectroscopic analytical technique (coating method) was used to analyze the free ligand and the complexes. The SEM image and EDX micrograph of the chelate and the complexes are shown in Figure 15(A–D). The surface morphology of the free ligand shows rod-like glassy material, and after coordination with the metal ions, the $Cr^{3+}$ complex displayed wide block surface morphology. The $Co^{2+}$ and $Zn^{2+}$ complexes showed spherical surface morphology. The transformation in the surface morphology of the free ligand compared with that of the complexes further confirmed the emergence of the complexes. Furthermore, the EDX micrographs revealed the chemical composition of the complexes and fully supported the complexes' proposed structures. In addition, the presence of the chloride and nitrate as counter ions in the $Cr^{3+}$ and $Co^{2+}$ complexes was also confirmed by the EDX micrograph of the complexes, Figure 16.

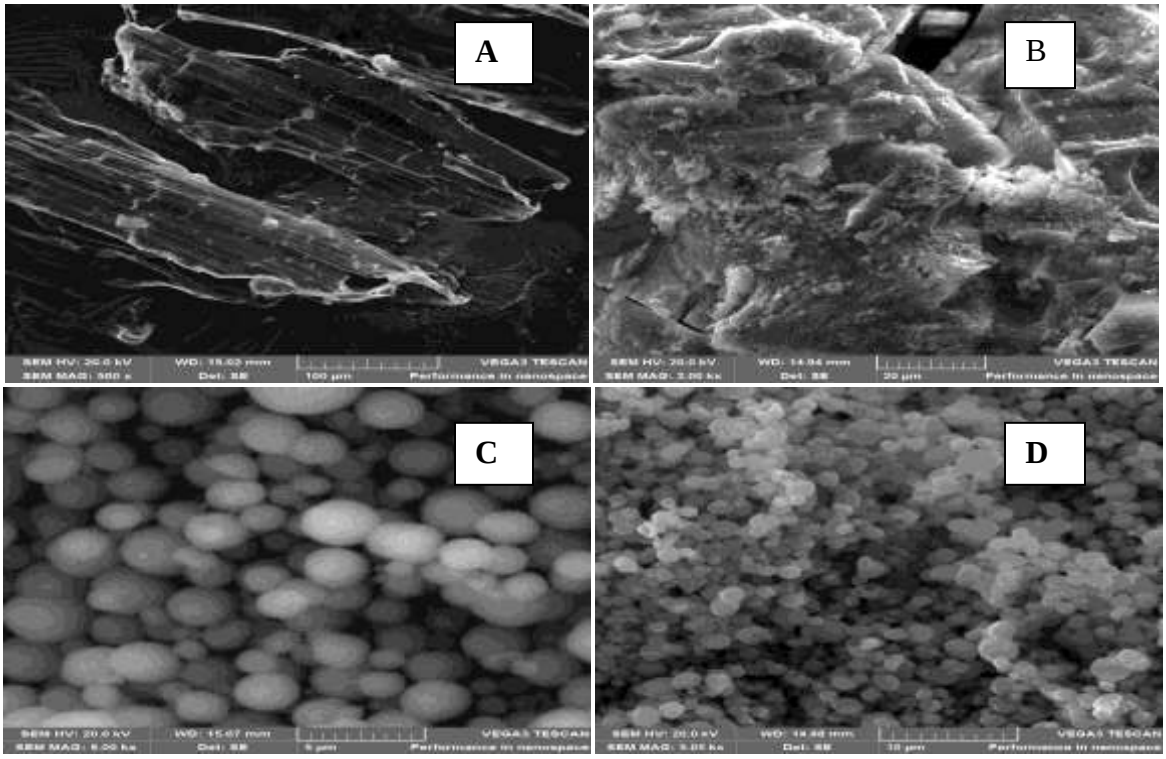


**Figure 15:** SEM images of the ligand and the complexes: A = Ligand, B = $[Cr(IM)_2(H_2O)_2]$, C = $[Co(IM)_6]Cl_2$, and D = $[Zn(IM)_2(H_2O)_2]$

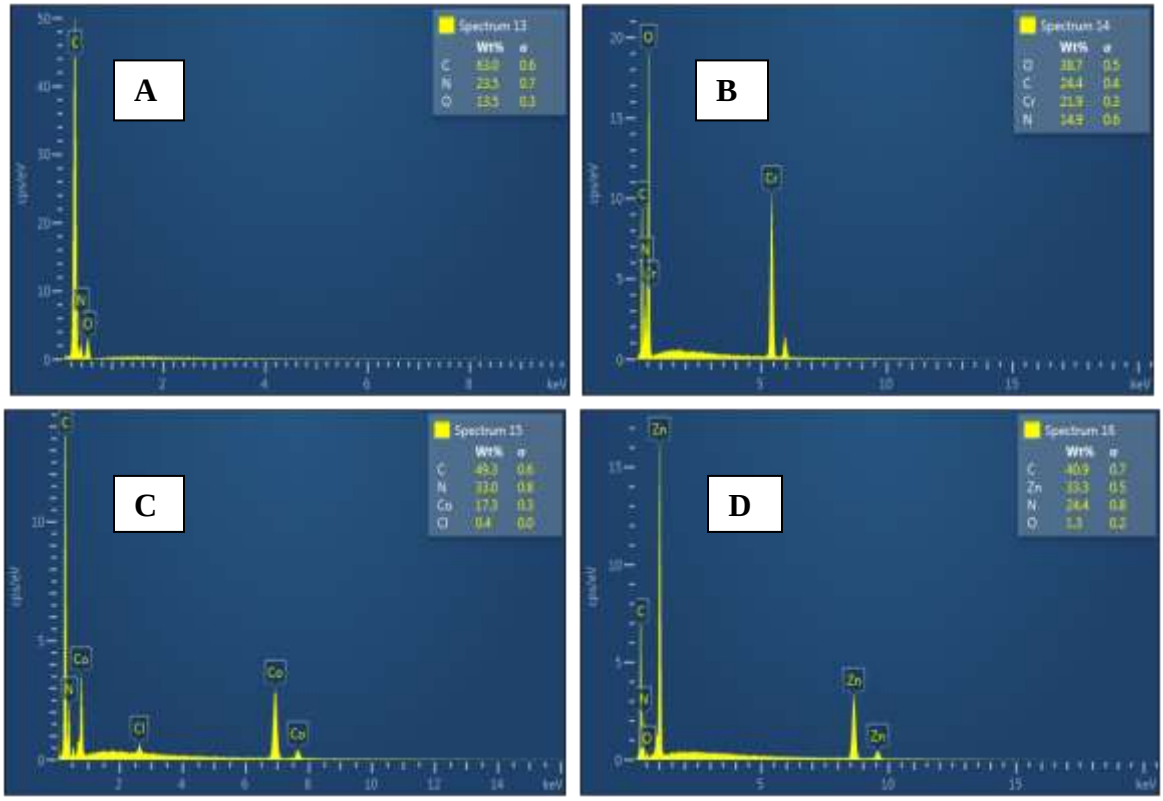


**Figure 16:** EDX micrograph of the ligand and the complexes: A = Ligand, B = $[Cr(IM)_2(H_2O)_2]$, C = $[Co(IM)_6]Cl_2$, and D = $[Zn(IM)_2(H_2O)_2]$

**Structure of the complexes**

From the data generated on the different characterization techniques deployed to establish and validate the complex formation, the stoichiometry and structural orientation of the compounds are presented in **Scheme 2.**

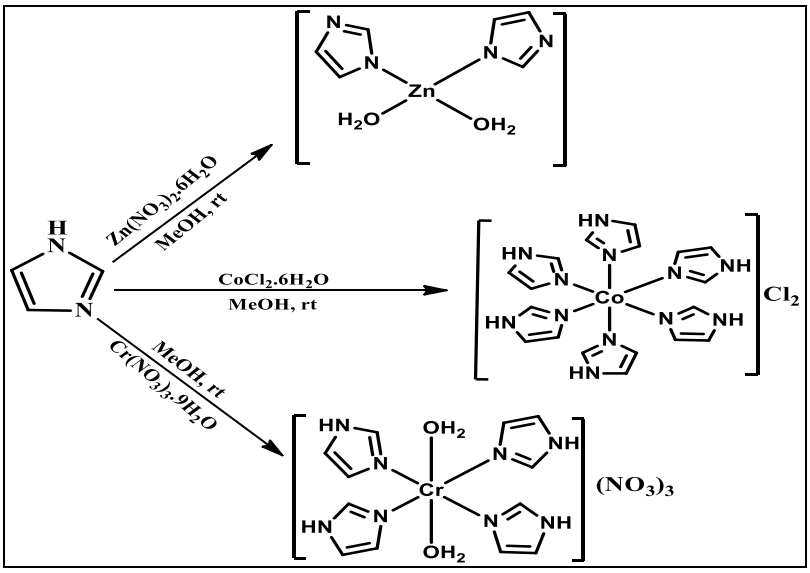


**Scheme 2:** Proposed structures of the synthesized complexes

**Cyclic voltammetry studies**

Cyclic voltammetry (CV) evaluated the redox activity of the synthesised complexes of $Cr^{3+}$, $Co^{2+,}$ and $Zn^{2+}$ with the imidazole ligand. The redox behavior of metal ions is an important determinant of their biological activity. Redox-active metals show better biological activity compared to redox inactive metals. Therefore, this study was performed to ascertain the redox behavior of the metal complexes and compare them with their antimicrobial study. The $Zn^{2+}$ complex cyclic voltammograms were performed at a scan rate of 50 mV/s in 0.01M PBS (pH=7.4), as shown in Figure 18A. The complex shows neither oxidative nor reductive waves in the potential range of -0.5 to 2.0 V. This means the $Zn^{2+}$ complex isn't electro-active. The diamagnetic property of the $Zn^{2+}$ complex, which lacks an unpaired electron, could explain the electro-inactivity.

Figure 18B and C shows the CV of $Cr^{2+}$ and $Co^{2+}$ complexes in a 0.01 M PBS electrolyte at various scan rates (20, 40, 60, 80 mV/s). In the potential range of -0.5 to 2.0 V, the two complexes display a reductive wave. The reduction peak can be assigned to the reduction process of $Cr^{3+}$ to $Cr^{2+}$ and $Co^{2+}$ to $Co^{+}$. This suggests that the $Cr^{3+}$ to $Cr^{2+}$ and $Co^{2+}$ to $Co^{+}$ systems are irreversible one-electron systems (Gosser, 1993). Figure 18D representing the ligand's CV shows a comparable electrochemical response to $Cr^{3+}$ and $Co^{2+}$ complexes with a reduction peak denoting a reduction involving one-electron transfer.

The reliance of peak potential on scan rates implies that just one electron is transferred. A plot of reduction peak currents, $I_{pc}$ against scan rates, *v* was plotted as shown in insets of Figure 1B, C, and D for the $Cr^{3+}$ and $Co^{2+}$ complexes and the ligand. The plots were found to be linear, suggesting the electrode process was controlled by adsorption (Zhang & Anson, 1992).

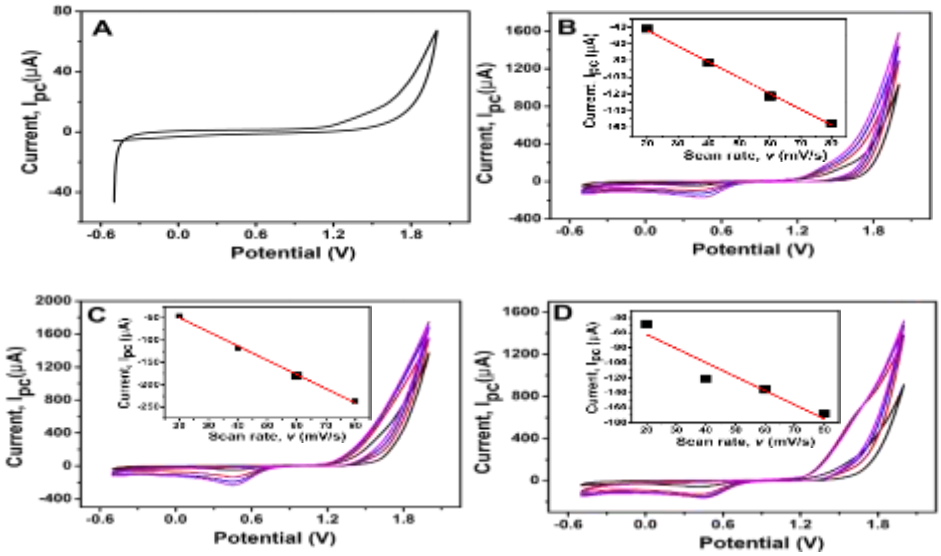


**Figure 18:** Cyclic voltammograms of (A) $[Zn(IM)_2(H_2O)_2]$ at scan rate of 50 mV/s in 0.01 M PBS pH 7.4, (B) $[Cr(IM)_4(H_2O)_2]$, inset: Calibration curve of $I_{pa}$ versus *v*, (C) $[Co(IM)_6]Cl_2$, inset: Calibration curve of $I_{pa}$ versus *v*, (D) Imidazole Ligand, inset: Calibration curve of $I_{pa}$ versus *v*. The scan rate is 20, 40, 60 and 80 mV/s in 0.01 M PBS pH 7.4

**Antimicrobial activity**

Antibacterial activity of the free ligand and the metal complexes were screened against Gram-positive strains (*S. aureus* ATCC-2593 and *S. pyogene* ATCC-19615) and Gram-negative strains (*E. coli* ATCC-25922 and *K. pneumoniae* ATCC-13883) using *in vitro* disc diffusion method, with a concentration of 10 and 20 mg/mL of the compounds. DMSO and ciprofloxacin were used as negative and positive controls, respectively. The data obtained were recorded in Table 4 and Figure 19–20, and the representative culture plates are shown in Figure 21. From this result, it can be seen that the free ligand demonstrated less antimicrobial activity on all the pathogens compared to the complexes. Furthermore, the metal complexes showed less antimicrobial activity than the positive control (ciprofloxacin). The antimicrobial activity shown by the ligand could be ascribed to the existence of hydrogen bonding between the imidazole proton and with active center of the bacterial cell wall. This altered the normal cellular process and thereby resulting in death (Alomar, Khan, Allain, & Bouet, 2009). The increase in the antimicrobial activity upon coordination with the metal ions can be corroborated based on the principle of chelation theory. According to the chelation theory, when ligands chelate metal ions, it results in the decrease in the polarity of the metal ion significantly due to the overlapping between the orbital of the ligand with that of the metal ion, and enable it to have more stability for eased of interference with cellular activity (Al-Amiery, Al-Majedy, Ibrahim, & Al-Tamimi, 2012; Hashem et al., 2021). Furthermore, metals have been used as antimicrobial agents since time immemorial (Lemire, Harrison, & Turner, 2013). However, some of these metals are toxic and can easily cause harm when used directly as a drug. But chelation with ligand minimizes the toxic effect of the metals because of geometry stabilization (Haas & Franz, 2009). In addition, the ability of a metal to participate in redox reaction enhances its biological activity and allows metals to transfer electrons as part of an important biological process. Redox-active metals can influence biological processes and can easily distrust biological mode of action (Ma, Jacobsen, & Giedroc, 2009). It is evident from the antimicrobial results that $Cr^{3+}$ and $Co^{2+}$ complexes showed better activity than the $Zn^{2+}$ complex, which confirms the result of cyclic voltammetry studies conducted on the complexes that say $Cr^{3+}$ and $Co^{2+}$ were found to be redox-active while $Zn^{2+}$ is redox inactive. Therefore, the results of cyclic voltammetry studies correlate well with antimicrobial studies results.

**Table 4:** The results of the antimicrobial studies of the ligand and its complexes

| Compound | Conc. (mg/mL) | Zone of inhibition (mm) | | | |
|---|---|---|---|---|---|
| | | ***S. aureus*** | ***S. Pyogenes*** | ***E. coli*** | ***K. pneumoniae*** |
| IM | 10 | 7 ±0.07 | 6±0.07 | 5±0.11 | 5±0.09 |
| | 20 | 13±0.15 | 11±0.08 | 12±0.06 | 9±0.23 |
| $[Cr(IM)_4(H_2O)](NO_3)_3$ | 10 | 14±0.14 | 11±0.017 | 8±0.08 | 12±0.08 |
| | 20 | 26±0.07 | 24±0.23 | 21±0.14 | 19±0.09 |
| $[Co(IM)_6]Cl_2$ | 10 | 18±0.11 | 15±0.19 | 11±0.09 | 14±0.12 |
| | 20 | 33±0.23 | 28±0.05 | 24±0.25 | 24±0.14 |
| $[Zn(IM)_2(H_2O)_2]$ | 10 | 12±0.13 | 9±0.06 | 7±0.05 | 8±0.10 |

| | | | | | |
|---|---|---|---|---|---|
| | 20 | 22±0.05 | 20±0.24 | 17±0.17 | 15±0.23 |
| Ciprofloxacin | 10 | 24±0.20 | 16±0.014 | 17±0.05 | 16±0.16 |
| | 20 | 39±0.17 | 33±0.23 | 30±0.01 | 28±0.25 |
| DMSO[b] | 20 | NA | NA | NA | NA |

NA = no activity; the values presented are the mean of the three closely related experimental values. [b]DMSO is included as a negative control based on its usage as a solvent carrier for the test compounds.

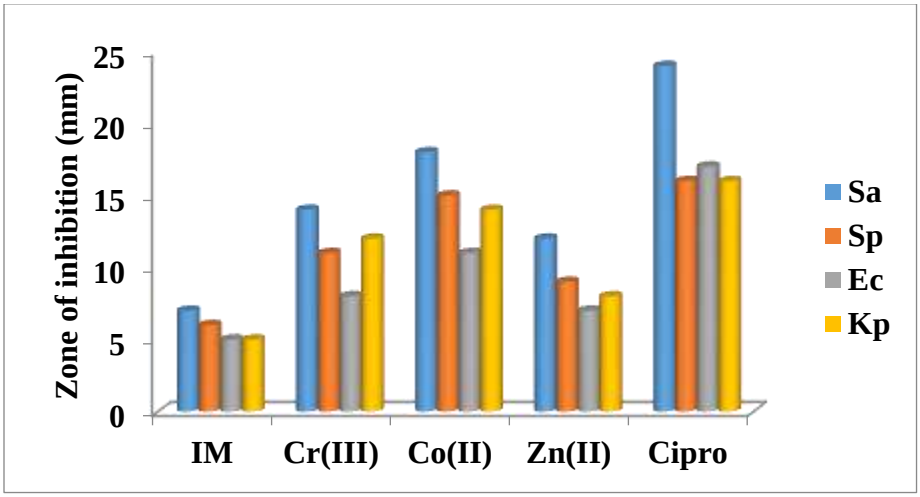


**Figure 19:** A histogram showing the result of antimicrobial activity of the ligand at its complexes at conc. of 10 mg/mL. Sa = *Staphylococcus aureus*, Sp = *Streptococcus pyogenes*, Ec = *Escherichia coli*, Kp = *Klebsiella pneumoniae* and Cipro = Ciprofloxacin

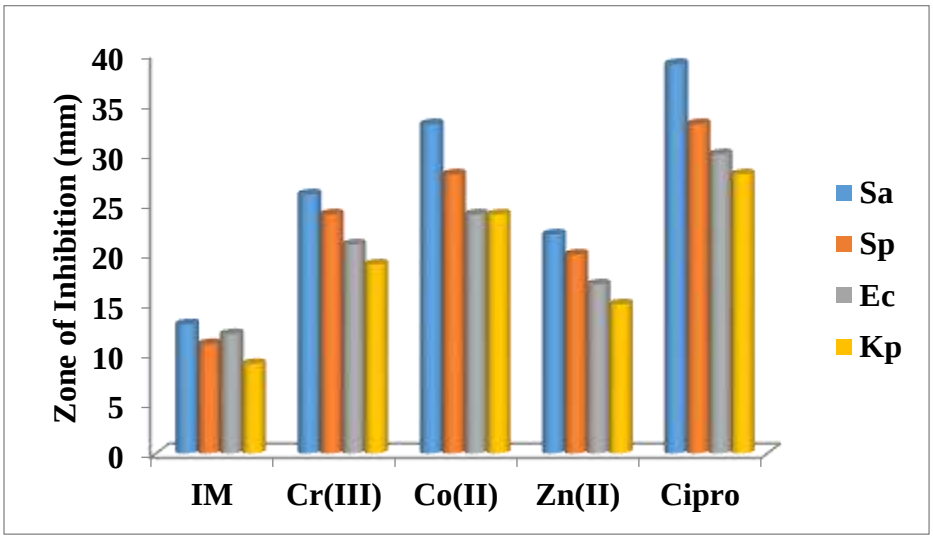


**Figure 20:** A histogram showing the result of antimicrobial activity of the ligand at its complexes at conc. of 20 mg/mL.

**Figure 21:** The representative culture plates showing the zone of inhibitions of the compounds against the bacteria

## CONCLUSION

Complexes of $Cr^{3+}$, $Co^{2+,}$ and $Zn^{2+}$ derived from 1*H*-imidazole were successfully synthesised and characterised. The stoichiometry and structures of the complexes were unveiled using FTIR, UV-Vis, elemental-CHN, HRMS, PXRD, TGA, SEM-EDX, and $^{1}H$ and $^{13}C\{H\}$NMR for the diamagnetic $Zn^{2+}$ complex. The data obtained from the characterization revealed that the ligand act as monodentate and coordinates through the nitrogen atom. The $Cr^{3+}$ and $Co^{2+}$ were found to have octahedral geometry and tetrahedral geometry for the $Zn^{2+}$ complex. The PXRD spectroscopic data indicated that $Co^{2+}$ and $Zn^{2+}$ complexes are crystalline, while $Cr^{3+}$ is amorphous in nature. Cyclic voltammetry studies showed that complexes of $Cr^{3+}$ and $Co^{2+}$ are redox-active, and $Zn^{2+}$ is redox inactive. *In vitro* antibacterial studies showed that the complexation of the metal ions to ligand increases the antimicrobial activity on all the tested bacteria. $Co^{2+}$ complexes demonstrated higher antimicrobial activity than $Cr^{3+}$ and $Zn^{2+}$ complexes. The results obtained present a good case for additional work on these substances as viable candidates for targeted bacteria.

### Authors' contribution statement

The authors listed here were fully involved in the conceptualization of the study, data generation, authentication, examination, and evaluation of the manuscript.

### Declaration of competing interest

The authors declare no conflict of interest

## REFERENCES

Al-Amiery, A. A., Al-Majedy, Y. K., Ibrahim, H. H., & Al-Tamimi, A. A. (2012). Antioxidant, antimicrobial, and theoretical studies of the thiosemicarbazone derivative Schiff base 2-(2-imino-1-methyl imidazolidine-4-ylidene) hydrazinecarbothioamide (IMHC). *Organic and medicinal chemistry letters, 2*(1), 1-7.

Alamanova, E., Shyytyeva, N., Berdalieva, Z., Abdyldaeva, N., Duishonbaeva, A., & Abdullaeva, Z. (2021). Coordination Polymer of Cobalt (II) Nitrate with Imidazole: Synthesis, Properties, and Crystal Structure. *Journal of*

*Crystallization Process and Technology*, *10*(1), 1-9.

Alomar, K., Khan, M. A., Allain, M., & Bouet, G. (2009). Synthesis, crystal structure, and characterization of 3-thiophene aldehyde thiosemicarbazone and its complexes with cobalt (II), nickel (II), and copper (II). *Polyhedron*, *28*(7), 1273-1280.

Alzahrani, S., Morad, M., Bayazeed, A., Aljohani, M. M., Alkhatib, F., Shah, R., . . . Zaky, R. (2020). Ball milling approach to preparing new Cd (II) and Zn (II) complexes; characterization, crystal packing, cyclic voltammetry, and MOE-docking agrees with the biological assay. *Journal of Molecular Structure*, *1218(3)*, 128473-12882.

Andersson Trojer, M., Movahedi, A., Blanck, H., & Nydén, M. (2013). Imidazole and triazole coordination chemistry for antifouling coatings. *Journal of Chemistry*, 6(2), 119-126.

Bai, S. Q., Young, D. J., & Hor, T. A. (2011). Nitrogen-Rich Azoles as Ligand Spacers in Coordination Polymers. *Chemistry–An Asian Journal*, *6*(2), 292-304.

Basner, A. D. (2017). *Synthesis of heteroaromatic ruthenium dyes for use as electron reservoirs in dye-sensitized solar cells.* Syracuse University.

Bhuiyan, A. A., Kudo, S., & Bartlett, J. (2010). Synthesis and characterization of ruthenium complexes containing chlorophenanthroline and bipyridine. *Journal of the Arkansas Academy of Science*, *64*(1), 33-40.

Chen, S.-S. (2016). The roles of imidazole ligands in coordination supramolecular systems. *CrystEngComm*, *18*(35), 6543-6565.

Constable, E. C., & Housecroft, C. E. (2019). The early years of 2, 2′-bipyridine—a ligand in its lifetime. *Molecules, 24*(21), 3951-3962.

Dalal, M. (2017). *A Textbook of Inorganic Chemistry–Volume 1*: Dalal Institute.

Davison, T. W. (2014). Ruthenium complexes of new heterocyclic ligands. *Biorganic Chemistry, 8, 340-354.*

Ding, P., Wang, Y., Kou, H., Li, J., & Shi, B. (2019). Synthesis of heterobinuclear Cu (II)-Ni (II) complex: Structure, CT-DNA interaction, hydrolytic function, and antibacterial studies. *Journal of Molecular Structure, 1196*, 836-843.

Erden, I. b., Demirhan, N., & Avcıata, U. (2006). Synthesis and characterization of a new imidazole ligand and its complexes with cobalt (II), nickel (II), and copper (II). *Synthesis and Reactivity in Inorganic, Metal-Organic and Nano-Metal Chemistry*, *36*(7), 559-562.

Fischer, N. (2010). *Novel Ligands based on Imidazole and Triazole: From Coordination Chemistry to Medicinal Applications and Material Design.* Friedrich-Alexander-Universität Erlangen-Nürnberg (FAU).

Gonon, M. (2020). Case Studies in the X-ray Diffraction of Ceramics.

Gosser, D. K. (1993). *Cyclic voltammetry: simulation and analysis of reaction mechanisms* (Vol. 43): VCH New York.

Groom, C. R., Bruno, I. J., Lightfoot, M. P., & Ward, S. C. (2016). The Cambridge structural database. *Acta Crystallographica Section B: Structural Science, Crystal Engineering and Materials*, *72*(2), 171-179.

Haas, K. L., & Franz, K. J. (2009). Application of metal coordination chemistry to explore and manipulate cell biology. *Chemical reviews*, *109*(10), 4921-4960.

Hashem, H. E., Mohamed, E. A., Farag, A. A., Negm, N. A., & Azmy, E. A. (2021). New heterocyclic Schiff base-metal complex: Synthesis, characterization, density functional theory study, and antimicrobial evaluation. *Applied Organometallic Chemistry*, e6322.

Hassan, F. S., Fayez, M., & Abdalla, N. (2020). Coordination Behavior and Biological Activity of Some Transition Metal Complexes with 2-Acetyl and 2-Formyl-3-Amino-1, 4-Naphthoquinone Ligands. *Open Journal of Inorganic Non-metallic Materials*, *10*(02), 15-23

Karaağaç, D. (2020). Spectroscopic and thermal studies of cyano bridged hetero-metallic polymeric complexes derived from ligands containing N and S donor atoms. *Bulletin of the Chemical Society of Ethiopia*, *34*(2), 365-376.

Kerru, N., Gummidi, L., Maddila, S., Gangu, K. K., & Jonnalagadda, S. B. (2020). A review on recent advances in nitrogen-containing molecules and their biological applications. *Molecules*, *25*(8), 1909-1918.

Lemire, J. A., Harrison, J. J., & Turner, R. J. (2013). Antimicrobial activity of metals: mechanisms, molecular targets and applications. *Nature Reviews Microbiology*, *11*(6), 371-384.

Ma, Z., Jacobsen, F. E., & Giedroc, D. P. (2009). Coordination chemistry of bacterial metal transport and sensing. *Chemical reviews*, *109*(10), 4644-4681.

Othman, I. M., Gad-Elkareem, M. A., El-Naggar, M., Nossier, E. S., & Amr, A. E.-G. E. (2019). Novel phthalimide based analogues: Design, synthesis, biological evaluation, and molecular docking studies. *Journal of enzyme inhibition and medicinal chemistry*, *34*(1), 1259-1270.

Pal, S. (2018). *Pyridine: A useful ligand in transition metal complexes*: IntechOpen.

Qi, Y., & Wang, Y. (2014). Five new Mn (II) complexes based on flexible bis (imidazole) ligands: Synthesis, structure and magnetic properties. *Polyhedron*, *73*, 133-138.

Richardson, C. (1999). Synthesis and Complexes of Heterocyclic Ligands.

Sandbhor, U., Kulkarni, P., Padhye, S., Kundu, G., Mackenzie, G., & Pritchard, R. (2004). Antimelanomal activity of the copper (II) complexes of 1-substituted 5-amino-imidazole ligands against B16F10 mouse melanoma cells. *Bioorganic & Medicinal Chemistry Letters*, *14*(11), 2877-2882.

Sridharan, K. (2016). *Spectral methods in transition metal complexes*: Elsevier.

Trivedi, M. K., Branton, A., Trivedi, D., Nayak, G., Saikia, G., & Jana, S. (2018). Physical and structural characterization of biofield treated imidazole derivatives. *Natural Products Chemistry & Research*, *3*(5), 1000187.

Tyagi, P., Chandra, S., Saraswat, B., & Yadav, D. (2015). Design, spectral characterization, thermal, DFT studies and anticancer cell line activities of Co (II), Ni (II) and Cu (II) complexes of Schiff bases derived from 4-amino-5-(pyridin-4-yl)-4H-1, 2, 4-triazole-3-thiol. *Spectrochimica Acta Part A: Molecular and Biomolecular Spectroscopy*, *145*, 155-164.

Uluçam, G., & Turkyilmaz, M. (2018). Synthesis, structural analysis, and biological activities of some imidazolium salts. *Bioinorganic chemistry and applications, 2018*.

Yan, N., Zhao, Y.-F., Niu, L.-Q., Zhou, C.-S., Liu, Y.-L., He, T., . . . Yue, K.-F. (2017). Synthesis and structures of a series of d10 coordination compounds based on flexible bis (imidazole) ligand and dicarboxylates. *Inorganic and Nano-Metal Chemistry, 47*(6), 925-933.

Zhang, J., & Anson, F. C. (1992). Voltammetry and in-situ Fourier transform IR spectroscopy of two anthraquinone disulfonates adsorbed on graphite electrodes. *Journal of Electroanalytical Chemistry, 331*(1-2), 945-957.